Pergamon

Scripta Materialia, Vol. 40, No. 7, pp. 873–878, 1999
Elsevier Science Ltd

1359-6462/99/$–see front matter

PII S1359-6462(99)00046-9

PRECIPITATION HARDENING IN ALUMINUM ALLOY 6022

W.F. Miao and D.E. Laughlin
Department of Materials Science and Engineering, Carnegie Mellon University,
Pittsburgh, PA 15213, USA

(Received July 10, 1998)
(Accepted in revised form January 21, 1999)

Introduction

The use of aluminum alloys for automotive body materials has been driven by a number of issues, in particular weight reduction. The heat treatable Al-Mg-Si alloys of the 6xxx series are often chosen for these applications, since they show a good combination of formability, corrosion resistance and weldability [1]. The strengthening of Al-Mg-Si alloys is based on a precipitation hardening process. The precipitation sequence in the Al-Mg-Si alloys is generally accepted [1–3] to be:

$$\alpha \text{ (sss)} \rightarrow \text{GP zones} \rightarrow \beta'' \rightarrow \beta' \rightarrow \beta$$

where α (sss) is the supersaturated solid solution, GP zones are generally considered spherical clusters with unknown structure. The β'' are fine needle-shaped zones along $<100>_{Al}$, with a monoclinic structure (different values of the lattice parameters were reported [2,3]), and β' are rod-shaped precipitates (circular cross sections) along $<100>_{Al}$, having a hexagonal crystal structure with a = 0.705 nm and c = 0.405 nm [2,4]. However, other lattice parameters for β' have also been reported [5]. The β phase are usually Mg_2Si platelets on {100} of Al having the fcc CaF_2 structure with a = 0.639 nm [4].

Although the precipitation process in Al-Mg-Si alloys has been extensively studied, the understanding of the hardening process is still incomplete, since any change in composition, processing and aging practices etc. could affect the precipitation hardening behavior. In this paper, hardness measurements, differential scanning calorimetry and transmission electron microscopy have been utilized to study the precipitation hardening behavior in aluminum alloy 6022.

Experimental Procedure

The composition of the 6022 alloy used in this study is given in Table 1. The alloys were cast, homogenized, hot and cold rolled to 1.9 mm sheets. The sheet samples were solution treated for 20 min at 560°C and quenched in ice water. Artificial aging was carried out at a temperature of 175°C to imitate the paint bake temperature used in automotive applications. All specimens were quenched to room temperature at the completion of aging. In one set of samples, the interval between solution treatment and artificial aging was limited to a few minutes or less. In another set of samples, the alloy was naturally aged for 30 days prior to artificial aging.

TABLE 1
Actual Compositions of the 6022 Alloy

Alloy	Mg (wt%)	Si (wt%)	Fe (wt%)	Cu (wt%)	Mn (wt%)	A1 (wt%)
6022	0.58	1.28	0.11	0.07	0.08	balance

Six Rockwell 15T hardness measurements were taken and averaged for each of the samples. Differential scanning calorimetry (DSC) analysis was carried out in a Perkin-Elmer DSC-2 at a heating rate of 10°C/min. During DSC measurements, the samples were protected with flowing argon. A high purity Al sample of the similar mass to that of the specimen was used as a reference. Transmission electron microscopy (TEM) was performed in a Philips TM420 microscope operating at 120 kV. TEM specimens were prepared by jet-polishing in 30 vol% HNO_3 - 70 vol% CH_3OH solution at −20 to −30°C.

Results and Discussion

Figure 1 presents the DSC curve obtained at a heating rate of 10°C/min for the 6022 alloy immediately after solutionizing and quenching. The DSC curve showed four exothermic peaks and one large endothermic peak. The four exothermic peaks were centered near 95°C (peak I), 240°C (peak II), 290°C (peak III) and 335°C (peak IV), respectively. The endothermic peak (V) appeared at around 515°C.

To reveal to which precipitation reactions the peaks on the DSC curve in Figure 1 correspond, TEM observations were made on samples annealed in the DSC at a heating rate of 10°C/min to temperatures just above the corresponding peaks. For the sample heated just above the DSC peak I, no ordered precipitates were observed by TEM. Comparison with previous results suggests that DSC peak I is probably related with the formation of GP zones [6,7].

Figure 2 shows the TEM micrographs of a sample heated just over peak II (~ 260°C). The bright field image revealed strain contrast of needle-like precipitates oriented along $[010]_{Al}$ and $[100]_{Al}$ directions together with some fine dots. The needles were typically 20–40 nm long. Most of the dots should be the end-on sections of the needles along $[001]_{Al}$. The dark-field image showed that the diameter of the needles was in the range of 2–5 nm. The selected area diffraction pattern showed faint streaks along $[010]_{Al}$ and $[100]_{Al}$ due to the needle-like precipitates [4,8]. This indicates that DSC peak II corresponds to the precipitation of β''.

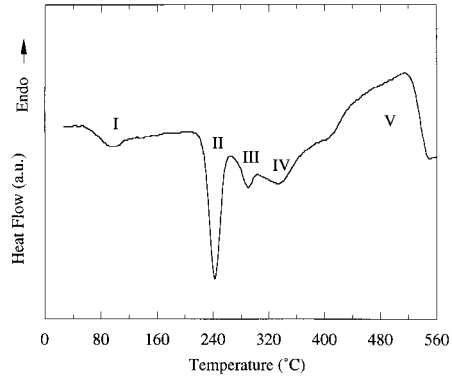

Figure 1. DSC trace of an as-quenched sample taken at a scan rate of 10°C/min.

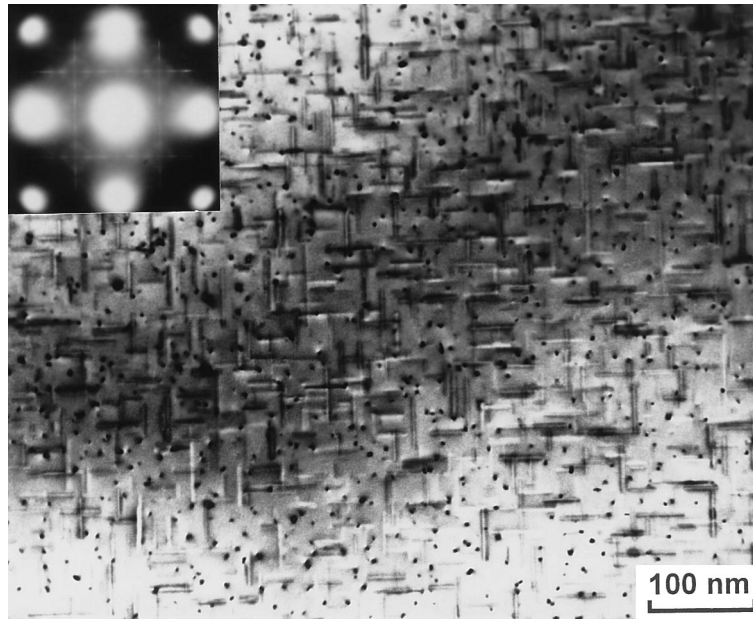

Figure 2. Bright-field TEM micrographs ($[001]_{Al}$ zone axis) of the sample heated to 260°C at 10°C/min immediately after solutionizing and quenching. Needle-like β'' precipitates oriented along $<010>_{Al}$ directions are observed.

Figure 3 shows the microstructure of a sample heated just over DSC peak III in Figure 2. At first sight, some rod-like precipitates with different diameters were observed along $[010]_{Al}$ and $[100]_{Al}$ directions. However, close examination of the end-on section of these precipitates revealed rectangle shape in addition to round shape. The round-shape was due to β' which is considered rod-like. The rectangle-shape suggested that the corresponding precipitates were lath-like. The appearance of lath-like precipitates were previously reported in Al-Mg-Si(-Cu) alloys [9–12]. Although the determination of the crystal structure of the lath-like precipitates is still under investigation, the analysis of the diffraction pattern in Fig. 3 suggests that the crystal structure of the lath-like precipitates observed in this study is very close to B′ reported in reference [10]. Chakrabarti et al. [11] have suggested that this phase be denoted as Q.

The microstructure of a sample heated to 377°C (end of DSC peak IV in Figure 1) was also examined. Large particles with different morphologies and a few large rods were observed. Energy dispersive spectroscopy and microdiffraction analysis showed that they were either β-Mg_2Si or Si, suggesting that the DSC peak IV corresponds to the precipitation of β and Si. Consequently, the broad endothermic peak (peak V) on the DSC curve in Figure 1 is most likely caused by the dissolution of the β and Si.

Figure 4 shows the hardness as a function of artificial aging time for samples with and without natural aging. For samples without natural aging, the hardness increased with aging time up to 500 min. After that, the hardness decreased slightly. For the artificial aging condition most interesting to the automotive industry (about 175°C for 20 min), the alloy was still under-aged. As expected, the naturally aged sample exhibited higher initial hardness when compared with samples which had not been naturally aged. However, the naturally aged sample showed a decrease in hardness upon initial artificial aging. Then, the hardness began to increase to a slightly higher peak hardness than samples which had not been naturally aged. It should be noted that after 20 min at 175°C, the hardness of the naturally aged sample was lower than that of the sample without natural aging.

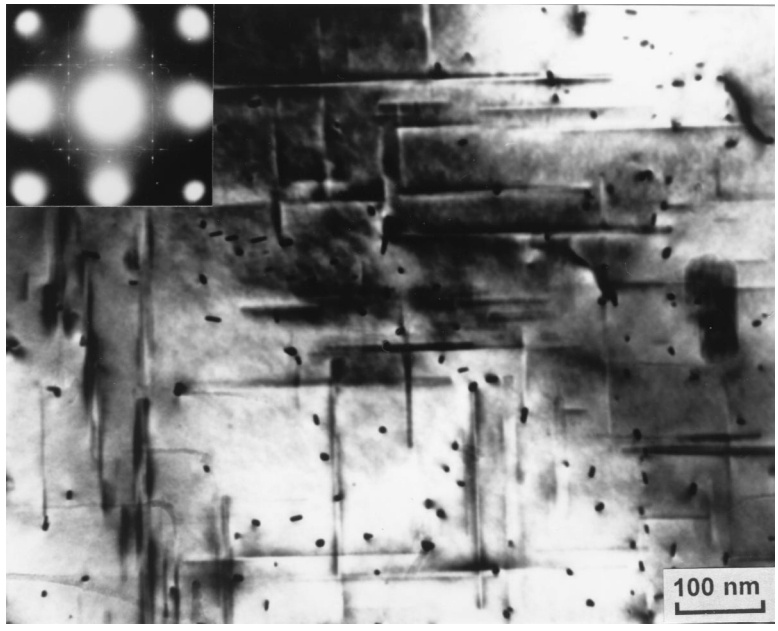

Figure 3. Precipitation morphology ($[001]_{Al}$ zone axis) of the sample heated to 300°C at 10°C/min immediately after solutionizing and quenching. At this stage, rod-like and lath-like precipitates predominate.

The detrimental effect of natural aging on precipitation hardening has been reported previously [12,13], and is thought due to the fact that the clusters formed during natural aging consume the vacancies and solute atoms and are hard to redissolve. It is clear from the present study that the initial decrease of hardness for the naturally aged sample (see Figure 1) was attributed to the reversion of GP zones formed during natural aging. On the other hand, it seemed that natural aging had little effect on prolonged aging at 175°C. This is contrary to the effect of natural aging on the artificial aging at a similar temperature in an Al-Mg-Si alloy, where even lower peak hardnesses were observed [12].

Figure 5 shows the microstructure of a sample aged at 175°C for 1000 min which was slightly over-aged. The microstructure was very similar to that shown in Fig. 2. This indicates that β'' is the main strengthening phase in 6022 alloys.

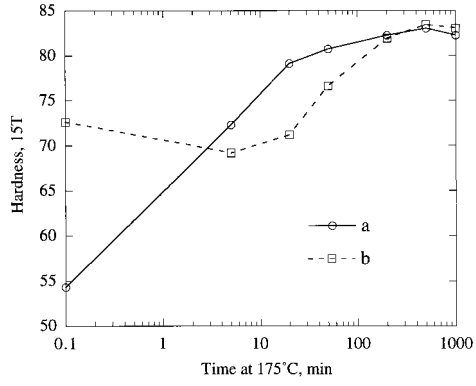

Figure 4. Dependence of hardness on artificial aging time at 175°C. (a) without natural aging; (b) 30 days of natural aging.

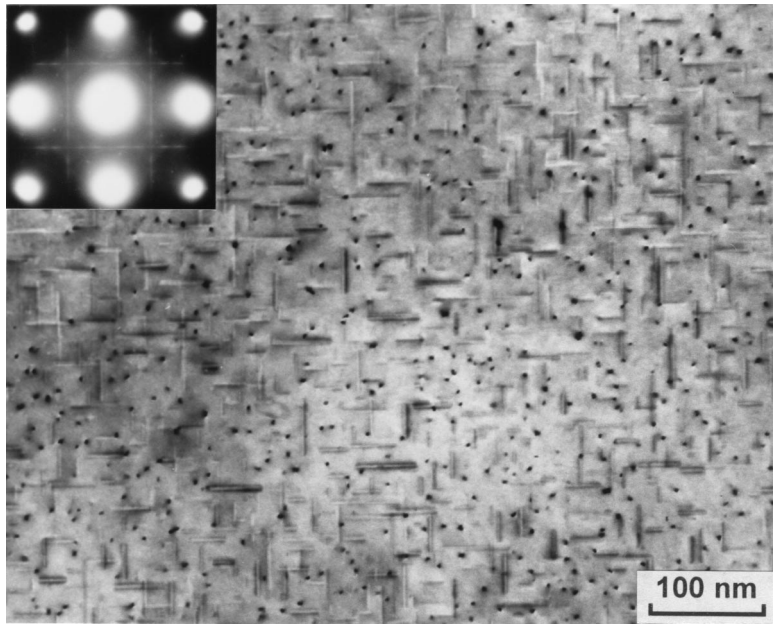

Figure 5. Microstructure ($[001]_{Al}$ zone axis) of the sample artificially aged at 175°C for 1000 min without natural aging. Comparison with Fig. 2 suggests that the precipitates are β''.

In Figure 6 the DSC plots for a sample naturally aged for 30 days and a sample artificially aged at 175°C for 1000 min are displayed. Compared with the DSC curve in Figure 1, it is seen that the exothermic peak around 95°C (peak I) disappeared on both of the DSC curves in Figure 6. For the naturally aged sample, it seemed that an endothermic peak was present at around 215°C, overlapping with the exothermic peak at 247°C. Two exothermic peaks also presented at around 290°C and 345°C, corresponding to peak III and IV in Figure 1, respectively. Another endothermic peak appeared at around 518°C. Since for solution treated samples, the DSC peak I and peak II (see Figure 1) correspond to the formation of GP zones and β'' respectively, it is not difficult to understand the DSC traces in Figure 6. The disappearance of peak I on the DSC curves of the naturally aged sample indicates that

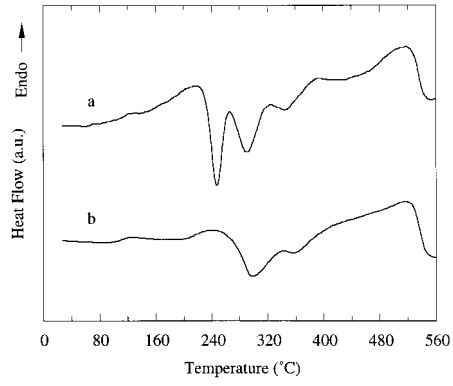

Figure 6. DSC curves at a scan rate of 10°C/min for samples (a) naturally aged for 30 days and (b) artificially aged at 175°C for 100 min without natural aging.

either GP zones already existed in the sample. For the sample artificially aged at 175°C for 1000 min, it is not surprising to see the disappearance of both peak I and peak II since β'' precipitates were already in the sample (Fig. 5). The endothermic peak at 215°C in Figure 6a was caused by the reversion of the GP zones and the exothermic peak at 245°C in Figure 6b should be due to the dissolution of β''. Comparison of Fig. 6a with Fig. 1 revealed that the peak temperature for the DSC peak corresponding to the precipitation of β'' was slightly higher in naturally aged alloy than in as-quenched alloy. This may help explain the sluggish aging kinetics in the naturally aged alloy (see Fig. 4).

Summary

Based on the results of DSC measurements and TEM observations, we suggest that the precipitation sequence in aluminum alloy 6022 be as follows: α(sss) $\rightarrow$ GP zones $\rightarrow$ needle-like β'' $\rightarrow$ rod-like β' + lath-like precipitates $\rightarrow$ β + Si with various morphologies.

During artificial aging at 175°C, the hardening in alloy 6022 is mainly caused by the precipitation of needle-like β''. The hardness of the alloy without natural aging increases with increasing aging time. A relatively long aging time is required to reach peak hardness. Natural aging has a deleterious effect on the hardness of the alloy in the initial artificial aging stage but appears to increase the peak hardness slightly.

Acknowledgments

This research was initiated during a Sabbatical by DEL at the Alcoa Technical Center. The authors would like to thank Dr. L. M. Karabin, Dr. D. J. Chakrabarti and Dr. B. Lu for helpful discussions. WFM was partially supported by a grant from the Ford Motor Company. DEL acknowledges a grant from NEDO.

References

1. G. B. Burger, A. K. Gupta, P. W. Jeffrey, and D. J. Lloyd, Mater. Charact. 35, 23 (1995).
2. R. P. Wahi and M. von Heimendahl, Phys. Stat. Sol. (a). 24, 607 (1974).
3. S. J. Andersen, H. W. Zandbergen, J. Jansen, C. Treholt, U. Tundal, and O. Reiso, Acta Mater. 46, 3283 (1998).
4. M. H. Jacobs, Phil. Mag. 26, 1 (1972).
5. K. Matsuda, S. Tada, S. Ikeno, T. Sato, and A. Kamio, Scripta Metall. Mater. 32, 1175 (1995).
6. A. K. Gupta, P. H. Marois, and D. J. Lloyd, Mater. Sci. Forum. 217–222, 801 (1996).
7. J. D. Bryant, in Automotive Alloys, ed. S. K. Das, and G. J. Kipouros, p. 19, The Minerals, Metals & Materials Society, Warrendale, PA (1997).
8. G. Thomas, J. Inst. Metals. 90, 57 (1961–62).
9. K. Matsuda, S. Ikeno, T. Sato, and A. Kamio, Mater. Sci. Forum. 217–222, 707 (1996).
10. S. D. Dumolt, D. E. Laughlin, and J. C. Williams, Scripta Metall. 18, 1347 (1984).
11. D. J. Chakrabarti, B. K. Cheong, and D. E. Laughlin, in Automotive Alloys II, ed. S. K. Das, p. 27, The Minerals, Metals & Materials Society, Warrendale, PA (1998).
12. S. B. Kang, L. Zhen, H. W. Kim, and S. T. Lee, Mater. Sci. Forum. 217–222, 827 (1996).
13. D. W. Pashley, J. W. Rhodes, and A. Sendorek, J. Inst. Metals. 94, 41 (1966).